Electronic Supplementary Material (ESI) for Sustainable Energy & Fuels.

Gradient distribution of functional components in PAN-based electrolyte endowing solid-state lithium sulfur battery with long cycle life

Jizong Zhang [a,b], Yu Si [a,b], Qiumi Huang [a,b], Ting Yang [a,b], Chengyang Wang [a,b], Kemeng Ji [a,b], Jin Wang [c] and Mingming Chen [a,b]*

[a] Key Laboratory for Green Chemical Technology of MOE, School of Chemical Engineering and Technology, Tianjin University, Tianjin 300072, P. R. China

[b] Collaborative Innovation Center of Chemical Science and Engineering (Tianjin), Tianjin University, Tianjin 300072, P. R. China

[c] Sichuan Best Graphite New Energy Co., Ltd, Suining 629000, Sichuan, P. R. China

* E-mail: chmm@tju.edu.cn (Mingming Chen)

Experimental section

1 Materials and methods

The synthesis of MoP/MoS_2@C

MoP/MoS_2@C is synthesized according to the previous paper [1].

The preparation of PAN-based solid electrolyte

PAN, PMMA and other solid materials were dried at 80°C vacuum oven for over 24 h. Then, 0.1 g PMMA was dispersed into 10.0 g DMF at 50°C with continuous but slow stirring. About 3 h later, PAN (MW = 150,000) powder and 0.03 g super-P were added to the above solution subsequently. Until the uniform light-black solution was achieved, the as-obtained MoP/MoS_2@C was placed into. After stirring overnight, the thick solution was coated onto a clean glass pane with a doctor blade. The solid electrolyte layer could be obtained by experiencing a phase conversion process, that is, in detail, immersing the glass pane with electrolyte solution into water, then standing a few minutes, the electrolyte layer was automatically separated from the glass base. To condense such an electrolyte layer, it would be rolled immediately once fished out. There were four components in the solid electrolyte, naming PMMA, PAN, carbon (super-P), MoP/MoS_2@C. According to the distribution of each component in the electrolyte (from negative to positive electrode side), the electrolyte was named as *p*-PPCM (here *p* representing phase conversion). The control electrolyte is obtained by the similar method, without one or several components. They were *p*-PAN, *p*-PPm, *p*-PPmC, and *p*-PPmCMo. Besides, another control sample was prepared by coating PAN-based slurry onto glass pane and dried directly,

which was named as *c*-PAN and *c*-PPmCMo. Finally, the layer did not use as solid electrolyte until it sucked up a typical amount LiTFSI solution and evaporating all the solvents, named as *p*-PAN/Li, *p*-PPmLi, *p*-PPmCLi, *p*-PPmCMoLi and *c*-PAN/Li, *p*-PPmCMoLi.

2 Physical characterization

The field-emission scanning microscope (FESEM, S4800, Hitachi, Japan) with EDX was employed to exhibit the morphology and element distribution of the solid-state composite polymer electrolyte (CPE). The SSEs were conducted by X-ray diffraction (XRD) using a Bruker D8 Advanced X-ray diffractometer with Cu Kα radiation (at scanning step of 5^{o} min^{-1}) to get the crystallization behavior. Beyond XRD, polarizing microscope (Nikon Eclipse E600 Pol, Japan) and photograph of SSEs gave the detailed and visualized information. Differential scanning calorimetry (DSC, 200 F3, Netzsch, Germany, 5°C min^{-1}) and thermogravimetric analysis (TGA, TA-50 instrument) were performed in an N_2 atmosphere at 5°C min^{-1} to ensure the phase change and thermostability of SSEs. The BET specific surface area and pore structure of the SSEs were examined by a Tristar-3000 at 77 K. To get the content of sulfur species at the SSE surface next to either cathode or anode, X-ray photoelectron spectroscopy (PHI-1600 ESCA spectrometer) was performed.

3 Electrochemical measurements of the solid-state electrolyte

The ionic conductivity (σ)

The σ can be got by, firstly confirming the value of bulk resistance R of the cell that sandwiched the CPE between two stainless sheel sheets (SS, the diameter was 16

mm), then calculating by the following formula:

$$\sigma=L/SR$$

here the L and S represent the thickness (cm) and the area (cm^2) of the SS, respectively. As for the R values, they were obtained by the electrochemical impedance spectroscopy (EIS) test with an amplitude voltage of 10 mV in the frequency range from 10^6 to 10^{-1} Hz at temperatures from 30 to 70°C, which was conducted on CHI660E electrochemical work stations.

The electrochemical stability windows

The electrochemical stability window is exhibited as the stable voltage range of the cell assembled with stainless steel sheet, CPE and Li anode (SS|CPE|Li) in a linear scanning voltammetry (LSV) test at 50°C. The LSV curves had a voltage range of 1.0~6.0 V (*vs.* Li^+/Li) and a scanning rate of 1 mV s^{-1}. Note that the cells were assembled in the glove box.

The lithium ion migration number (t_{Li^+})

The t_{Li^+} can be calculated according to the following equation proposed by Vincent et al,

$$t_{Li^+} = \frac{I_t(\Delta V - I_0R_0)}{I_0(\Delta V - I_tR_t)} \times 100\%$$

where I_0 and I_t were the initial and steady (terminal) currents during the direct-current (DC) polarization (with a DC voltage of 10 mV) at 50°C, and the test object was Li|SSE|Li symmetric cells. The R_0 and R_t were the resistance values before and after the polarization measurement with the same system, but the technique is AC impedance in the frequency range from 10^6 to 10^{-1} Hz at temperature of 50°C, and

with an amplitude voltage of 10 mV.

The voltage polarization measurements

The polarization curves of various CPEs were generated with Li|CPE|Li cells on Land 2001A battery testing system by using galvanostatic charge/discharge technique. And the current density was 0.1 mA cm^{-2}.

4 Batteries assembly and electrochemical tests

Laboratory-scale all-solid-state cells were constructed by employing sublimed sulfur in combination with Super-P, binder and additive as the cathode, together with a lithium anode and a solid electrolyte located between the cathode and the anode. For composite cathode electrodes, it was prepared by mixing the slurry consisted of 70 wt.% sublimed sulfur, 20 wt.% super-P and 10 wt.% poly (vinylidene difluoride) (PVDF), then coating it onto an aluminum foil with a doctor blade. The mass loading of cathode is about 2.5~3.0 mg cm^{-2}, corresponding to a sulfur loading of 1.5~1.8 mg cm^{-2} in cathode. All the processes were performed in an argon filled glove box.

Electrochemical performances the all-solid-state lithium batteries (SSLSB) were investigated by galvanostatic charge/discharge tests at different C rate (1 C = 1675 mA g^{-1}) by using a multichannel battery test system (LAND CT-2001A, Wuhan Rambo Testing Equipment Co., Ltd.) under a cut-off voltage of 1.5~3.0 V. The temperature was controlled in a constant temperature oven. The specific capacities were calculated based on the mass of sulfur. CV and EIS were recorded on a CHI660E electrochemical work station.

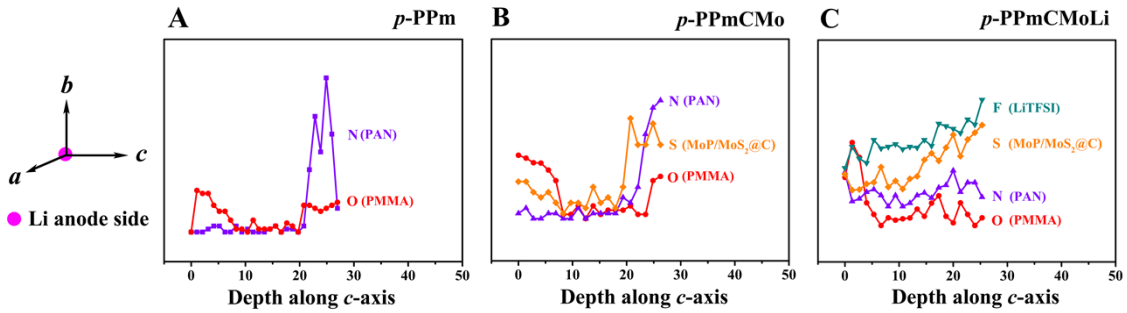

Figure S1 The elements/substances distribution of (A) *p*-PPm; (B) *p*-PPmCMo and (C) *p*-PPmCMoLi along *c*-axis.

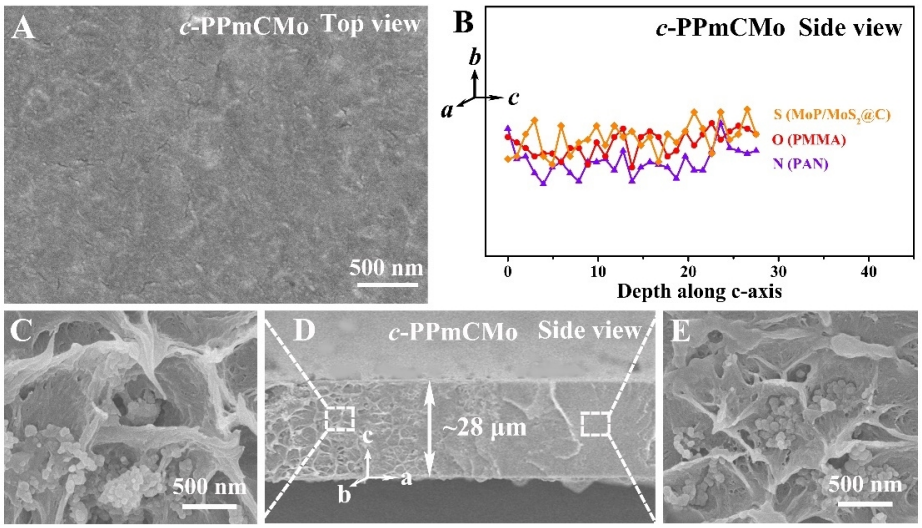

Figure S2 (A) FESEM image of the surface of *c*-PPmCMo membrane; (B) the elements/substances distribution of *c*-PPmCMo along *c*-axis; (D) cross-sectional micrographs of *c*-PPmCMo; (C) and (E) the enlarged and different areas of *c*-PPmCMo section.

The characterization of the *ab*- and *c*-axis section of the ungraded *c*-PPmCMo is shown in Figure S2. The composition is uniformly distributed. Compared with non-graded electrolytes, Grad-CPE exhibits different component distributions and functions at the cathode/electrolyte and anode/electrolyte interfaces, benefiting for both reaction and mass transfer.

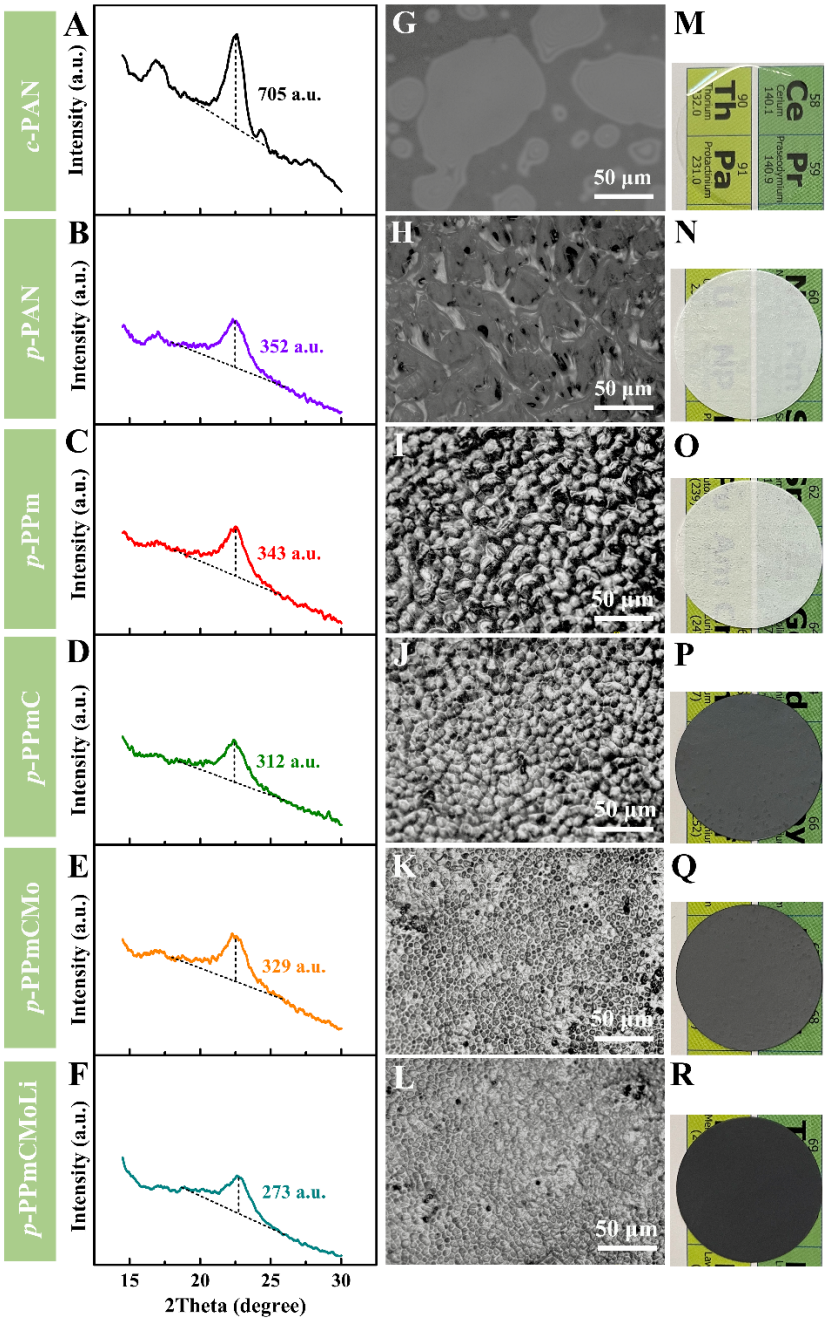

Figure S3 (A~F) XRD patterns; (G~L) polarizing microscope (POM) images and electronic photos of *c*-PAN, *p*-PAN, *p*-PPm, *p*-PPmC, *p*-PPmCMo and *p*-PPmcMoLi, respectively.

The crystallinity of the polymer segment in Grad-CPE is significantly reduced. The XRD peak intensity of p-PAN is only half of that of c-PAN, that is, it decreases from 705 a.u. to 352 a.u. (Figure S3A and S3B). The reduced intensity can be ascribed to

the following aspects: (1) The film forming temperature of *p*-PAN and *c*-PAN are different. Beyond the rigid and asymmetric structure, the high glass transition temperature (~94°C) and decomposition temperature (275°C) of PAN (Figure S4) make *p*-PAN have almost no rearrange and crystallize at the film forming temperature of 25°C; while the film formation of *c*-PAN occurs at 80°C, the generated energy enhances the possibility of polymer-chain movement, thus the crystallization ability increases. (2) The film forming speeds of *p*-PAN and *c*-PAN are different. The film formation of *p*-PAN is faster (about 40 s), but the movement speed of the polymer is so slow that the polymer cannot rearrange and crystallize in time during the film formation process, resulting in low crystallinity [2]; it takes above 2 h to get *c*-PAN. The crystallinity increases because long time makes the movement of polymer-chain possible. The addition of functional components basically maintains the crystallinity of Grad-CPE at the same or even smaller level (Figure S3C~F). The crystallinity of the *p*-PPmCMoLi is the lowest. Decrease in crystallinity means an increase in non-crystalline areas in polymer electrolytes, which is the main place for ion transfer and $S_8 \leftrightarrow Li_2S$ conversion.

The isotropy of the electrolyte membrane also benefits ion transport. As shown in Figure S3J~L, compared with other PAN-based electrolyte (Figures S3G and 4H), *p*-PPmCMoLi has the most uniform response to polarized light, indicating the most obvious isotropic characteristics on the *ab* surface of the membrane. The isotropic nature of the electrolyte on the *ab* plane means that its dielectric constant is scalar and has no directionality. Therefore, under the action of electric field force (during charge

and discharge), there is no restriction on the transmission direction of ions, and there are more transmission channels. Therefore, *p*-PPmCMoLi makes ions transport uniform and avoids local accumulation of ions, thus leading to excessive charge density and breakdown of the electrolyte. In addition, the diffuse reflectance of the *p*-PPmCMoLi film is enhanced, and the opacity increases (Figure 5-4M~R), indicating that (1) the arrangement of the polymer segments inside the electrolyte is irregular, the crystallinity is reduced, and (2) the surface/interface is rough, small pores appear. Both provide convenience for the transmission of ions [3]. Therefore, the reaction kinetics is increased from the perspective of increasing ion transport.

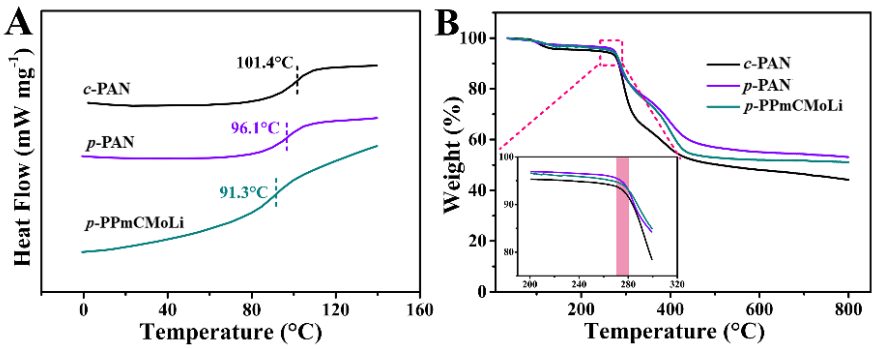

Figure S4 (A) DSC curves and (B) TG plots of c-PAN, *p*-PAN and *p*-PPmCMoLi.

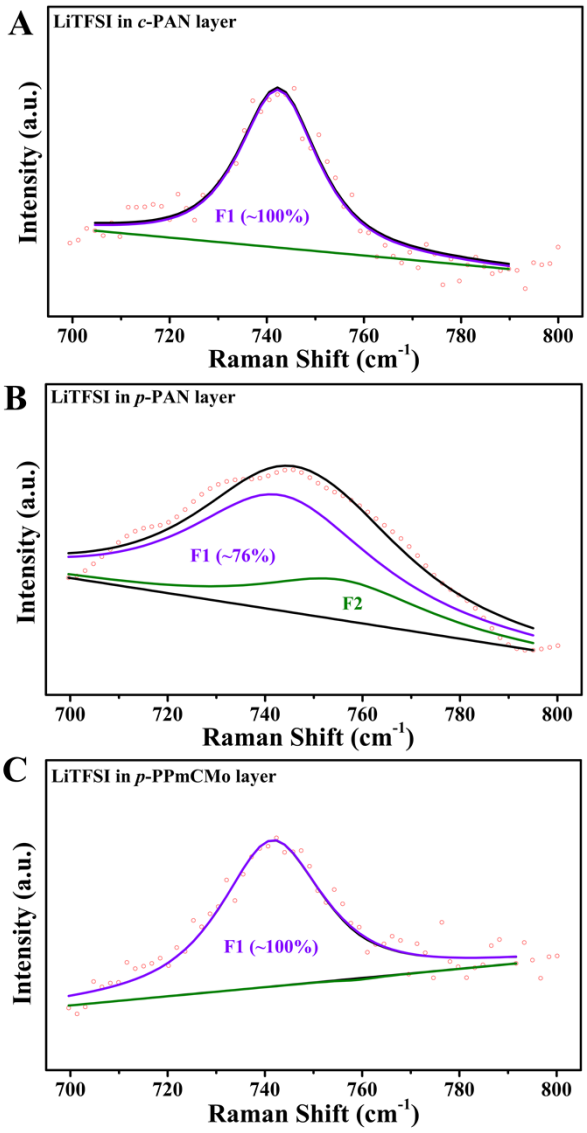

Figure S5 Raman spectra of (A) c-PAN/Li, (B) p-PAN/Li and (C) p-PPmCMoLi electrolyte.

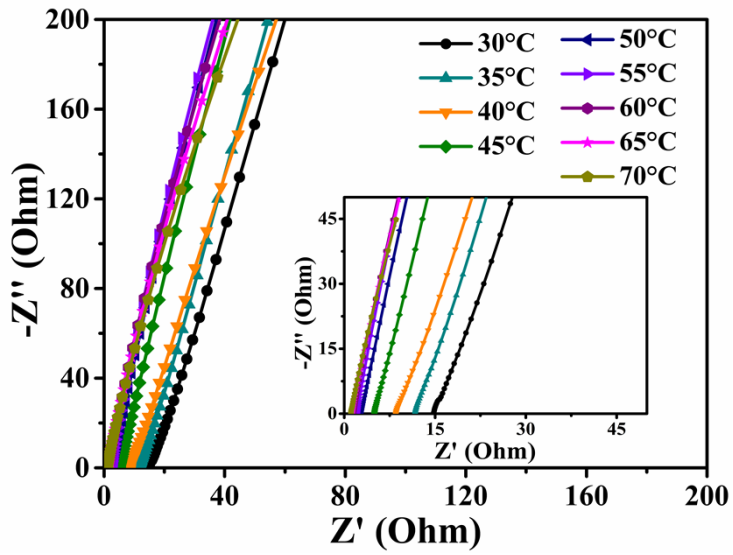

Figure S6 EIS spectrum of SS|*p*-PPmCMoLi|SS cell at a temperature range of 30~70°C.

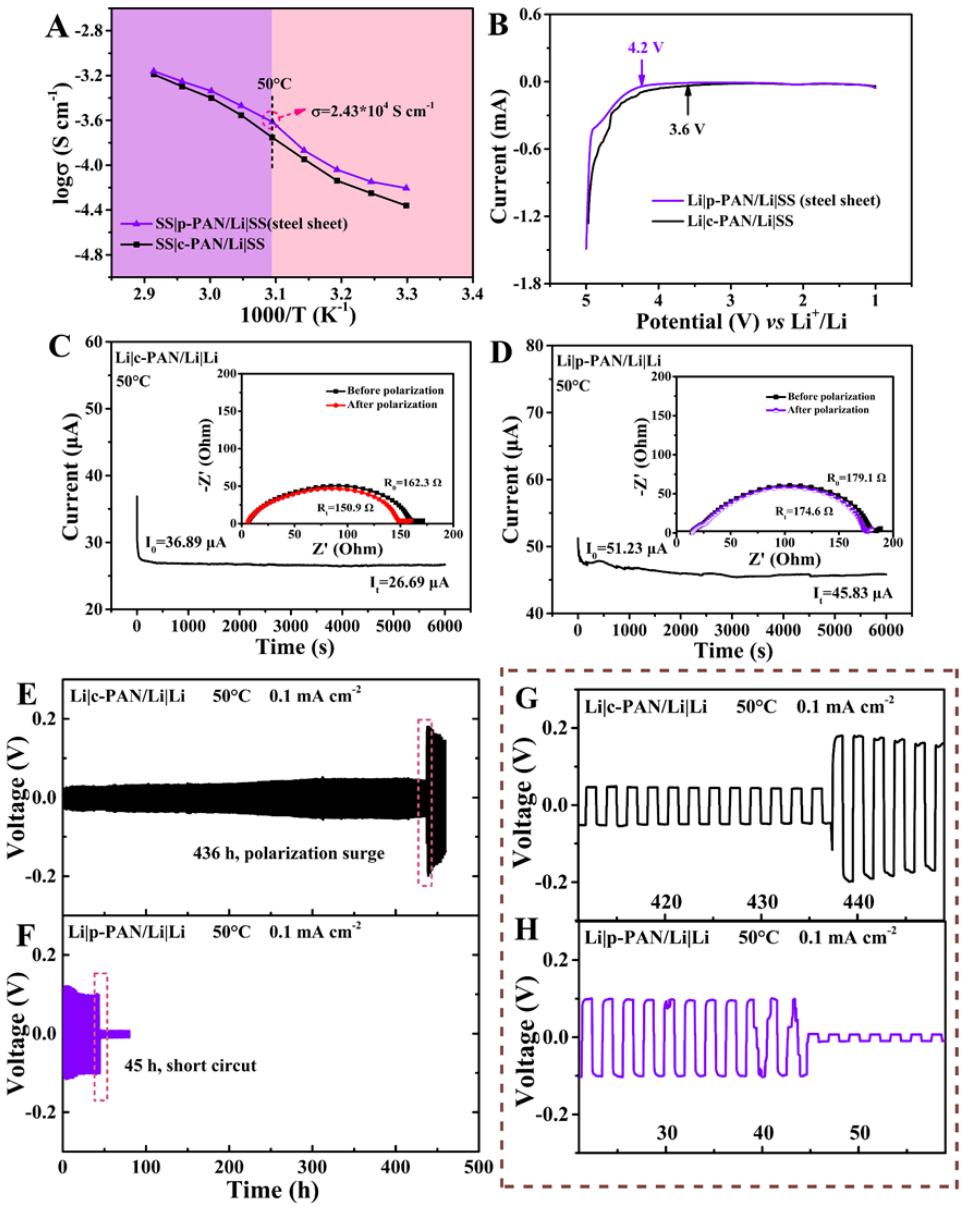

Figure S7 (A) Arrhenius plots of the *c*-PAN/Li and *p*-PAN/Li electrolytes; (B) LSV curves of Li|*c*-PAN/Li|SS and Li|*p*-PAN/Li|SS at 10 mV s^{-1}; Chronoamperometry profiles of (C) Li|*c*-PAN/Li|Li and (D) Li|*p*-PAN/Li|Li cells at 50°C (insets are the Nyquist impedance curves of the cells in their initial and stable polarization states). Galvanostatic cycling profiles (50°C) of (E) Li|*c*-PAN/Li|Li and (F) Li|*p*-PAN/Li|Li cells at 0.1 mA cm^{-2} and (G and H) the detail information of the selected regions in E and F, respectively.

In *p*-PAN/Li and *c*-PAN/Li symmetric cells (Li|CPE|Li), the ions at the electrode/CPE interfaces both transfer and react slowly, which is insufficient to maintain the fluent and complete Li^+ deposition/decomposition. In this case, the PAN-based electrolytes are subjected to a shock of aggregated ions and high voltage, they are much more vulnerable to experience short cycling life. As a consequence, the life span of *p*-PAN/Li cell comes to an end at only 45th hour (Figure S7E~H).

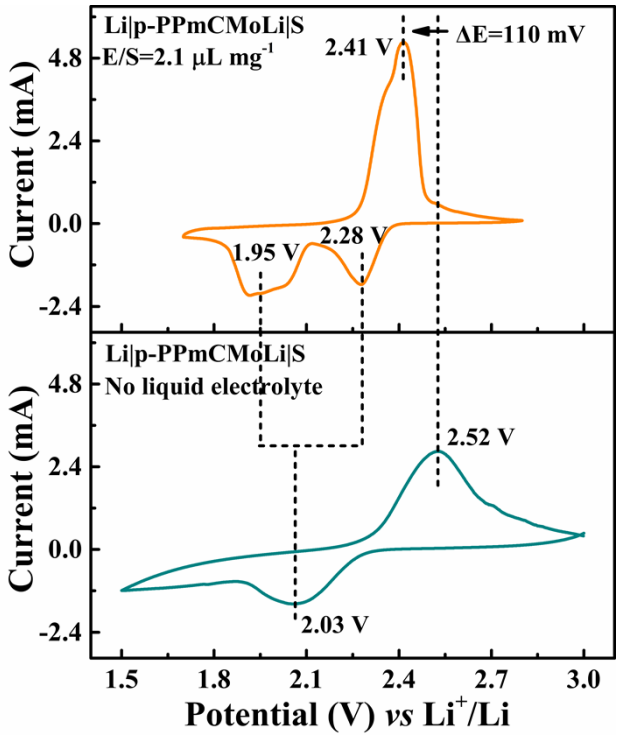

Figure S8 CV curves of Li|*p*-PPmCMoLi|S cell with a small amount (E/S = 2.1 μL mg^{-1}) of electrolyte be added or without electrolyte.

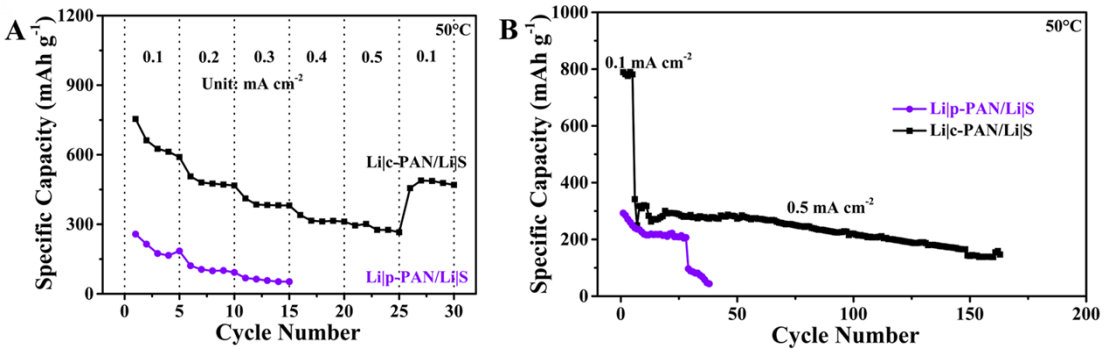

Figure S9 (A) Rate performances and cycling stabilities of Li|*c*-PAN/Li|S and Li|*p*-PAN/Li|S cells, the cycling of the two cells were tested at 0.5 mA cm^{-2} before 5-cycle activation at 0.1 mA cm^{-2}.

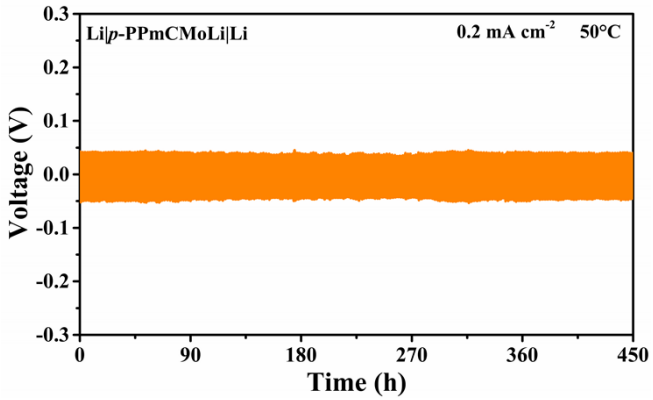

Figure S10 Galvanostatic cycling profiles of Li|*p*-PPmCMoLi|Li cells at 0.2 mA cm^{-2} and 50°C

Table S1 The solubility of different components in DMF and water.

	Dissolved form	Solubility (mg mL^{-1}) in different solvents	
		DMF (50°C)	**Water (25°C)**
PAN (MW = 150,000)	Swelling	~220	< 20
PMMA (MW = 150,000)	Swelling	~90	< 10
Super P	Dispersion	-	-
MoP/MoS_2@C	Dispersion	-	-

Table S2 The ionic-conductivity values of *c*-PAN/Li, *p*-PAN/Li, *c*-PPmcMoLi and *p*-PPmCMoLi electrolyte at a temperature range of 30~70°C.

Temperature (°C)	**Ionic Conductivity (S cm^{-1})**			
	***c*-PAN/Li**	***p*-PAN/Li**	***c*-PPmCMoLi**	***p*-PPmCMoLi**
30	4.36×10^{-5}	6.23×10^{-5}	5.38×10^{-5}	8.73×10^{-5}
35	5.62×10^{-5}	7.11×10^{-5}	6.39×10^{-5}	1.11×10^{-4}
40	7.26×10^{-5}	9.12×10^{-5}	7.45×10^{-5}	1.52×10^{-4}
45	1.13×10^{-4}	1.35×10^{-4}	9.24×10^{-5}	2.62×10^{-4}
50	1.76×10^{-4}	2.43×10^{-4}	1.30×10^{-4}	4.40×10^{-4}
55	2.79×10^{-4}	3.39×10^{-4}	1.59×10^{-4}	6.23×10^{-4}
60	3.98×10^{-4}	4.60×10^{-4}	2.09×10^{-4}	8.28×10^{-4}
65	5.04×10^{-4}	5.59×10^{-4}	3.04×10^{-4}	9.76×10^{-4}
70	6.48×10^{-4}	6.90×10^{-4}	3.98×10^{-4}	1.15×10^{-3}

Table S3 The relavent current and impendence values and the calculated t_{Li^+}.

	I_0 (μA)	I_t (μA)	R_0 (Ω)	R_t(Ω)	t_{Li^+}
***c*-PAN/Li**	36.89	26.29	162.3	150.9	0.17
***p*-PAN/Li**	51.23	45.83	179.1	74.6	0.26
***c*-PPmCMoLi**	32.30	19.51	116.2	113.5	0.17
***p*-PPmCMoLi**	77.93	71.06	110.9	109.2	0.65

Note: I_0 and I_t represent the current at initial and steady state during polarization. R_0 and R_t are the impedance before and after polarization

Table S4 The comparison of all solid-state LSBs electrolytes with their abbreviations

Abbreviation	Components
c-PAN or *p*-PAN	PAN
c-PAN/Li or *p*-PAN/Li	PAN + LiTFSI
p-PPm	PAN + PMMA
p-PCa	PAN + Super-P
p-PPmLi	PAN + PMMA + LiTFSI
p-PPmC	PAN + PMMA + Super-P
p-PPmCLi	PAN + PMMA + Super-P + LiTFSI
c-PPmCMo or *p*-PPmCMo	PAN + PMMA + Super-P + MoP/MoS_2@C
c-PPmCMoLi or *p*-PPmCMoLi	PAN + PMMA + Super-P + MoP/MoS_2@C + LiTFSI

Note: The prefix *c* represents the preparation method of the electrolyte membrane is coating-drying method, and *p* represents the phase inversion

Table S5 A performance comparison of symmetric solid-state battery tests

Solide electrolyte	Current (mA cm^{-2})	Cycle time (h)	Temperature (^oC)	Polarization voltage-Final (mV)	Reference
PEO-1%LSPS	0.1	600	60	25	S4
Vr/PEO-LCSE	0.05	200	60	14	S5
	0.1	200		26	
	0.2	200		47	
PLO	0.1	350	35	60	S6
PEO+Li3N	0.1	650	70	16	S7
SPE-LATP-SPE	0.25	220	75	50	S8
LiG3-LGPS	0.1	300	RT	43	S9
PLALF	0.05	200	60	9	S10
	0.1	200		16	
	0.2	200		34	
GPE@FEC	0.1	980	25	80	S11
LHB	0.1	1000	60	<100	S12
LEC	0.1	400	60	20	S13
p-PPmCMoLi	0.1	1000	50	30	This work

References

[1] Zhang J, Zhang J, Liu K, et al. Abundant defects-induced interfaces enabling effective anchoring for polysulfides and enhanced kinetics in lean electrolyte lithium-sulfur batteries. ACS Applied Materials & Interfaces, 2019, 11(50): 46767-46775.

[2] Nakamura K, Watanabe T, Katayama K, et al. Some aspects of nonisothermal crystallization of polymers. I. Relationship between crystallization temperature, crystallinity, and cooling conditions. Journal of Applied Polymer Science, 1972, 16(5): 1077-1091.

[3] Zhang X K, Xie J, Shi F F, et al. Vertically Aligned and Continuous Nanoscale Ceramic-Polymer Interfaces in Composite Solid Polymer Electrolytes for Enhanced Ionic Conductivity. Nano Letters, 2018, 18: 3829-3838.

[4] Li X, Wang D, Wang H, et al. Poly(ethylene oxide)-$Li_{10}SnP_2S_{12}$ Composite Polymer Electrolyte Enables High-Performance All-Solid-State Lithium Sulfur Battery. ACS Applied Materials & Interfaces, 2019, 11(25): 22745-22753.

[5] Zhai P, Peng N, Sun Z, et al. Thin laminar composite solid electrolyte with high ionic conductivity and mechanical strength towards advanced all-solid-state lithium–sulfur battery. Journal of Materials Chemistry A, 2020, 8(44): 23344-23353.

[6] Zhang Z, Zhao B, Zhang S, et al. A mixed electron/ion conducting interlayer enabling ultra-stable cycle performance for solid state lithium sulfur batteries. Journal of Power Sources, 2021, 487: 229428.

[7] Eshetu G G, Judez X, Li C, et al. Lithium Azide as an Electrolyte Additive for All-Solid-State Lithium-Sulfur Batteries. Angewandte Chemie, International Edition

in English, 2017, 56(48): 15368-15372.

[8] Wang Y, Wang G, He P, et al. Sandwich structured NASICON-type electrolyte matched with sulfurized polyacrylonitrile cathode for high performance solid-state lithium-sulfur batteries. Chemical Engineering Journal, 2020, 393: 124705.

[9] Cao Y, Zuo P, Lou S, et al. A quasi-solid-state Li–S battery with high energy density, superior stability and safety. Journal of Materials Chemistry A, 2019, 7(11): 6533-6542.

[10] Kou W, Wang J, Li W, et al. Asymmetry-structure electrolyte with rapid Li^+ transfer pathway towards high-performance all-solid-state lithium–sulfur battery. Journal of Membrane Science, 2021, 634: 119432.

[11] Zhang T, Zhang J, Yang S, et al. Facile In Situ Chemical Cross-Linking Gel Polymer Electrolyte, which Confines the Shuttle Effect with High Ionic Conductivity and Li-Ion Transference Number for Quasi-Solid-State Lithium-Sulfur Battery. ACS Applied Materials & Interfaces, 2021, 13(37): 44497-44508.

[12] Shi X, Zeng Z, Sun M, et al. Fast Li-ion Conductor of Li_3HoBr_6 for Stable All-Solid-State Lithium–Sulfur Battery. Nano Letters, 2021, 21(21): 9325-9331.

[13] Li M, Frerichs J E, Kolek M, et al. Solid-State Lithium–Sulfur Battery Enabled by Thio-LiSICON/Polymer Composite Electrolyte and Sulfurized Polyacrylonitrile Cathode. Advanced Functional Materials, 2020, 30(14): 1910123.